

123456789 123456789 123456789 123456789 123456789
123456789 123456789 123456789

X-ray analysis and matter distribution in the lens-cluster Abell 2390

M. Pierre¹, J.F. Le Borgne², G. Soucail², and J.P. Kneib^{2,3}

¹ CEA Saclay, Service d'Astrophysique, F-91191 Gif sur Yvette

² Observatoire Midi-Pyrénées, Laboratoire d'Astrophysique de Toulouse, URA 285, 14 Avenue E. Belin, F-31400 Toulouse

³ Institute of Astronomy, Madingley Road, Cambridge CB3 0HA, UK

Received ?? , Accepted ???

Abstract. We present a deep X-ray ROSAT/HRI observation of the rich cluster-lens Abell 2390 and the analysis of the gas and matter distribution in the cluster. The X-ray centroid coincides with the location of the central cD galaxy, and the core appears to be dominated by a massive cooling flow, one of the strongest ones ever studied. On larger scales, the X-ray distribution is elliptical and locally distorted by a significant “sub-structure” located some $100 h^{-1}$ kpc from the center. The mass of this sub-structure is estimated to be $\sim 1/20$ of the total cluster mass and appears to be associated with an enhancement in the galaxy distribution, in the region where the giant “straight arc” and several arclets are observed. A simple lens model based on the geometrical properties of the X-ray gas shows that this sub-structure allows to explain in a simple manner the peculiar shape of the arc and puts strong constraints on the total mass distribution in the central part of this cluster. The derived M/L in the central part of the cluster is found to be around 250 in solar units, a rather common value compared with other cluster-lenses. Moreover, the link between the matter distribution derived from the lens model and the density profile issued from the X-ray map analysis is used to infer the temperature profile in the cluster. This profile shows a significant decrease near the center, in agreement with the existence of the cooling flow. Both X-ray and lensing constraints are tied together to give a consistent picture of the dynamics of the central part of A2390.

Key words: Galaxies: clustering – Galaxies: cluster: individual Abell 2390 – Cosmology: observations – dark matter – gravitational lensing – X-rays: galaxies

1. Introduction

The problem of mass determination in clusters of galaxies is still a debated question although some significant advances have been recently achieved, often related to the improvement of the observing capabilities. So far, three independent methods are currently used to determine the mass distribution in galaxy clusters, each of them having its own limitations and uncertainties. First, the galaxy distribution combined with the

velocity dispersion gives the virial mass. Some more refined analysis of the velocity distribution are now explored (Merritt 1987; Merritt & Saha 1994; Merritt & Tremblay 1994). Secondly, the X-ray emission of the optically thin intracluster gas has long been thought to be the ideal tracer of the mass. Indeed, the collisional timescale of the ICM being much shorter than the Hubble time, one generally considers that the free-free emitting gas is in hydrostatic equilibrium in the cluster potential. Thus, the X-ray surface brightness of the cluster is simply related to the kinetic temperature of the gas and to the square of the electron density. The main difficulty arises while deprojecting the 2D X-ray map into a density profile, as this operation implicitly assumes spherical symmetry and requires in principle the knowledge of the temperature distribution.

The third approach is to use the gravitational lensing effect observed through rich and medium-distant clusters producing giant luminous arcs and arclets (Fort & Mellier 1994). The modelling of multiple arcs is a powerful tool to infer the central mass distribution and to constrain the core radius of the dark matter (e.g. Mellier et al. 1993; Kneib et al. 1993). From the analysis of several clusters, the estimated core radius seems about twice smaller than expected from the standard analysis of X-ray images (Kneib et al. 1995; Smail et al. 1995a); this discrepancy is not well understood yet, although probably due to the fact that, until very recently, the X-ray detector PSF has never been taken into account, so that published core radii are actually convolved values. Recent works (Loeb & Mao 1994; Miralda-Escudé & Babul 1995; Daines et al. 1995; Kneib et al. 1995; Allen et al. 1995) combine the X-ray and lensing analysis to study the dynamics of clusters. The morphology of the mass distribution inferred from the X-ray and lensing analyses agree and the mass centroid coincides with the brightest cluster galaxy (usually a cD or giant elliptical); the mass distribution having same orientation and ellipticity as the halo of the central galaxy. However, in some clusters such as A1689 and A2218, a discrepancy by a factor two in the mass estimates are noticed (Miralda-Escudé & Babul 1995). It can be explained by the fact that the cluster is merging and has not reach the state of hydrostatic equilibrium yet. On the contrary, in the cluster-lens PKS0745 (Allen et al. 1995) lensing and X-ray constraints do agree when a multiphase-model of the IGM (based on ROSAT/HRI and ASCA data) is used.

In this context, Abell 2390 ($z=0.232$) is an attractive object

Send offprint requests to: M. Pierre

to study in many respects: first, a “straight” giant gravitational arc has been detected by Pelló et al. (1991, hereafter Paper I) with its redshift measurement ($z=0.913$) and the identification of several arclets, indicating that the cluster may be massive and concentrated in its center. Moreover, the galaxy distribution presents an elongated shape, and the velocity dispersion $\sigma = 2112^{+274}_{-197}$ km s⁻¹ is quite large (Le Borgne et al. 1991, Paper II). This value may be overestimated by selection biases in the sample, and could be slightly reduced. Finally, strong evidences for a massive cooling flow arise from the detection of bright optical filaments in the envelope of the central cD galaxy, emitting low excitation emission lines, and a powerful unresolved radio source (Soucail et al. 1995, Paper IV). Einstein observation revealed a strong X-ray source (Ulmer et al. 1986), which when computed with the correct redshift corresponds to $L_X = 3.85 \cdot 10^{44} h^{-2}$ ergs s⁻¹ in the range 0.7–3.5 keV. This source is significantly elongated, with a centrally condensed core (Mc Millan et al. 1989). From its high X-ray luminosity and galaxy velocity dispersion, one may infer a large cluster mass; alternatively this could indicate that the cluster has not reached a relaxed state yet, in agreement with its overall very elongated morphology. This, together with the exceptional shape of the giant arc, may suggest the existence of a peculiar underlying gravitational potential as proposed by Kassiola et al. (1992). But despite the numerous arclets observed, a univoque modelling was not possible till now, because of the lack of lensing constraints within the Einstein radius. In the classical hypothesis where the hot emitting X-ray plasma is a much better tracer of the overall mass than the galaxies - which seems justified because of its considerably shorter mean free path - the gas distribution should be the most direct tool to discriminate between potential models derived from optical constraints alone. Thus, the need for a detailed mapping of the cluster central parts has motivated the obtention of a deep ROSAT HRI pointing which we analyse in this paper.

The paper is organised as follows. In Section 2, we present the X-ray and optical observations, as well as a morphological analysis of the maps and the significance of the different detected structures. Section 3 deals with the analysis of the gas properties derived from the X-ray flux and profile. In Section 4, the lensing properties of the cluster are examined in connection with the constraints derived from the gas distribution. The mass profile obtained from the lens modelling is then used to estimate the gas temperature profile. Finally, some conclusions on the matter distribution are given in Section 5. In all the paper we assume that $H_0 = 100 h$ km s⁻¹ Mpc⁻¹ ($0.5 < h < 1$), $\Omega_0 = 1$ and $\Lambda = 0$, which means that 1'' scales as $2.33 h^{-1}$ kpc at the cluster redshift; r and R stand respectively for the 3D and projected radial distances from the cluster center. Celestial coordinates are given in the J2000 reference system.

2. X-ray/optical morphological analysis

2.1. X-ray observations and optical re-centering

Pointed ROSAT HRI observations were obtained between November 23-25 1992, during a single exposure totalling 27764 sec. All processing of the X-ray data has been performed with the EXSAS/MIDAS package. The photon file was binned into a 1'' pixel image, and smoothed by a gaussian filter having a variable width function of the pixel intensities: from 5'' (nominal HRI FWHM) at the cluster center up to 20'' at the periphery; this enables to reduce the photon noise in the external

isophotes, without loosing spatial resolution in the brightest central region. Extended emission from the cluster is detected beyond 6' (i.e. at least $1 h^{-1}$ Mpc).

Figure 1 shows the X-ray contours overlaid on the cluster optical image. Absolute positioning of the X-ray image was directly obtained from the EXSAS image header, but the alignment of the optical image requires the precise knowledge of the cD coordinates which have to be determined relatively to surrounding known stars. The coordinates of the central galaxy published in Paper II have an uncertainty of about 2'' so we tried to improve the accuracy to better than 1''. The method we used consists in computing the transformation parameters between CCD coordinates and celestial coordinates with a least square minimisation on coordinates of stars of known equatorial coordinates measured on a CCD frame (in practice the Thuan-Gunn r image from the Isaac Newton Telescope described in Paper II). Because we do not have unsaturated stars of known coordinates on the CCD frames this was done in two steps:

- a) On a print of the Palomar Observatory Sky Survey (POSS) we measured the position of 22 stars of the HST Guide Star Catalogue in a field of about $15' \times 15'$ and computed the transformation parameters for the POSS print. At this point the standard deviation of the residuals is 0.7''. These parameters were then used to calculate the equatorial coordinates of 11 apparently stellar objects selected on a CCD frame where they appear unsaturated.
- b) The positions of these stellar objects were measured on the CCD frame. Their equatorial coordinates computed in a) were used to calculate the transformation parameters for the CCD frame. These parameters allowed to calculate the equatorial coordinates of the center of the central galaxy on the CCD frame. Although we did not improve the accuracy significantly, this second step was necessary because the position of the central galaxy was not well enough defined on the POSS print while it could be defined to within half a pixel (0.4'') on the CCD image.

The coordinates obtained for the central galaxy are: $\alpha_{2000} = 21^h 53^m 36.76^s$, $\delta_{2000} = 17^\circ 41' 42.9''$. The uncertainties are 0.04s in right ascension and 0.7'' in declination at a 99% confidence level. These coordinates are slightly different from those published in Paper II but they agree within uncertainties.

The X-ray emission is consistent with being centered on the cD galaxy within 1'' (the brightest pixel on the filtered image is at $\alpha_{2000} = 21^h 53^m 36.67^s$, $\delta_{2000} = 17^\circ 41' 43.7''$) provided that the absolute ROSAT attitude solution for this pointing is correct. The X-ray maximum appears extremely concentrated and peaked, suggesting the presence of a massive cooling flow, a first indication of the results discussed below.

2.2. Morphological analysis of the X-ray 2D distribution

On large scales, the X-ray image is strongly elliptical with an overall position angle comparable to the main cluster direction in the optical (i.e. galaxy distribution and cD major axis, see below). A conspicuous distortion of the isophotes due to an excess of emission is located some 40'' North-West from the cD and another one appears marginally on the opposite side of the cD (Fig. 1). In order to study the 2D distribution of the gas and the departure from a pure elliptical distribution, a detailed isophotal fit of the X-ray smoothed map was done, us-

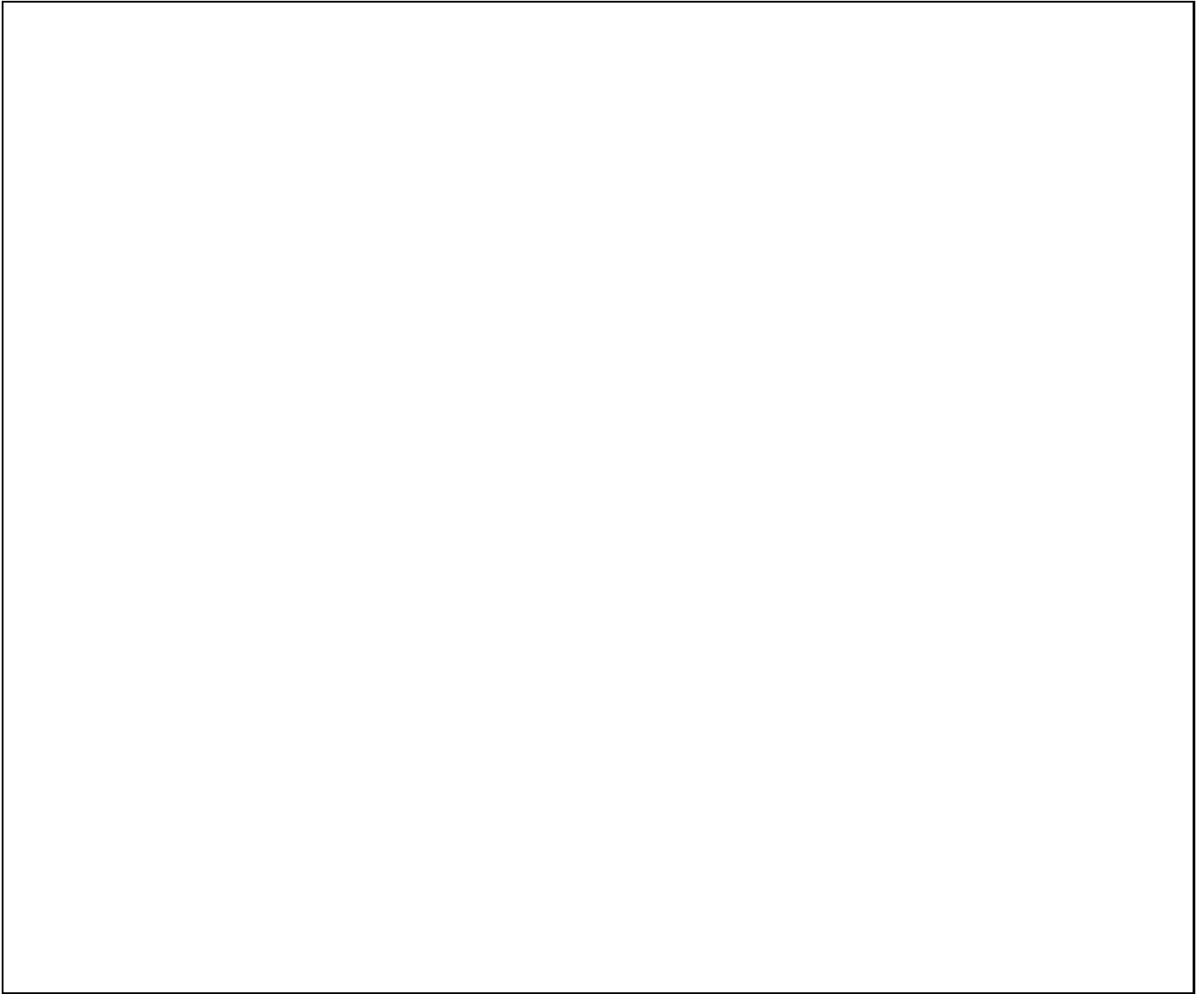


Fig. 1. Deep R-band image of A2390 obtained at the KPNO 4m telescope. The displayed field of view is $5' \times 5'$, centered on the cD galaxy. Overlaid are the ROSAT HRI contours equally separated in log space from 0.23 to 4.08×10^{-5} counts $\text{s}^{-1} \text{arcsec}^{-2}$. The X-ray image has been smoothed using a variable gaussian filter (see text).

ing the ELLIPSE package in the IRAF/STSDAS environment (Jedrzejewski 1987), as well as a wavelet analysis.

For the isophotal fit analysis, the two regions departing from a regular elliptical isophote were masked before the fit. Outside the central region, the fit was rather easy, with an increase of the ellipticity and a twist of the isophotes at large radius (Fig. 2). Near the center, there is also a strong rotation of the position angle of the isophotes and a significant decrease in the ellipticity for $R < 10''$. This may be due to some features at the very center, possibly poorly resolved with our data (see below, wavelet analysis) so that we did not consider residuals within the innermost $10''$. The elliptical model was subtracted to the initial X-ray map, and the residuals overlayed on the optical image (Fig. 3). In addition to the central residuals, three excess of emission are clearly visible on this map, noted P1, P2 and S. P1 and P2 appear unresolved while S is certainly

extended. In order to estimate the significance of each residual, we computed within each aperture the number of counts in the elliptical model and derived a signal-to-noise ratio of $S/N = N/\sqrt{N + N_{mod}}$. Their main morphological properties are summarised in Table 1.

As the process of subtracting a fitted ellipse implicitly assumes that the cluster has a perfect elliptical symmetry, and therefore may bias the significance of the residuals, we checked the above results independently, with a wavelet analysis of the central part of the X-ray image ($1''$ pixels not filtered). We used the method described by Slezak et al. (1994) and looked more specifically at two scales: $5''$ (HRI PSF) and $20''$. Results are displayed on Fig. 4.

For the smallest scale, the two point-like sources P1 and P2 are detected again, as well as a strong contribution from the cluster center identified with the core of the cooling flow

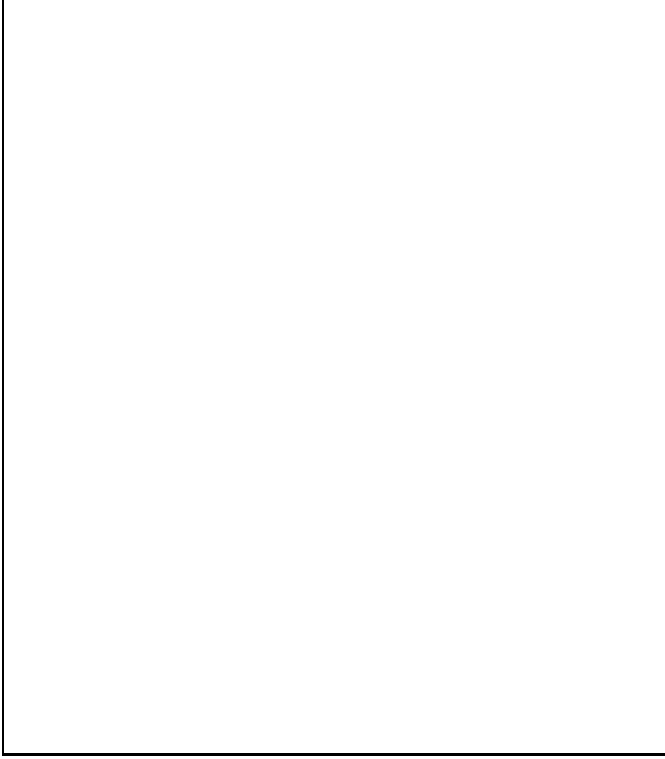


Fig. 2. Elliptical modelling of the X-ray image as a function of radial distance along the major axis. The squares correspond to the X-ray isophotes fit ($12'' < R < 120''$) and the crosses to the cD envelope fit, performed from the R CCD image ($2'' < R < 20''$). The upper graph represents the axis ratio distribution (b/a) and the lower one the position angle distribution of the major axis, measured counterclockwise from the North.

Table 1. Morphological properties of the residuals of the X-ray elliptical fit. Columns 2 and 3 give the offsets in RA and DEC from the cD galaxy, columns 4 gives the radial distance in kpc. In column 5, we estimate the significance of the excess (see text for more details), and in column 6 we give the relative intensity, scaled to the total cluster flux. Finally in column 7, we give the estimated X-ray luminosity, assuming a 2 keV temperature at the cluster redshift.

	$\Delta\alpha$ ($''$)	$\Delta\delta$ ($''$)	Distance (h^{-1} kpc)	S/N	F/F_{tot}	Luminosity (h^{-2} erg s^{-1})
P1	-17	+9	44	1.1	$3.4 \cdot 10^{-3}$	$1.6 \cdot 10^{42}$
P2	-24	-9	61	1.8	$5.4 \cdot 10^{-3}$	$2.6 \cdot 10^{42}$
S	-37	-25	105	2.6	$9.0 \cdot 10^{-3}$	$4.4 \cdot 10^{42}$

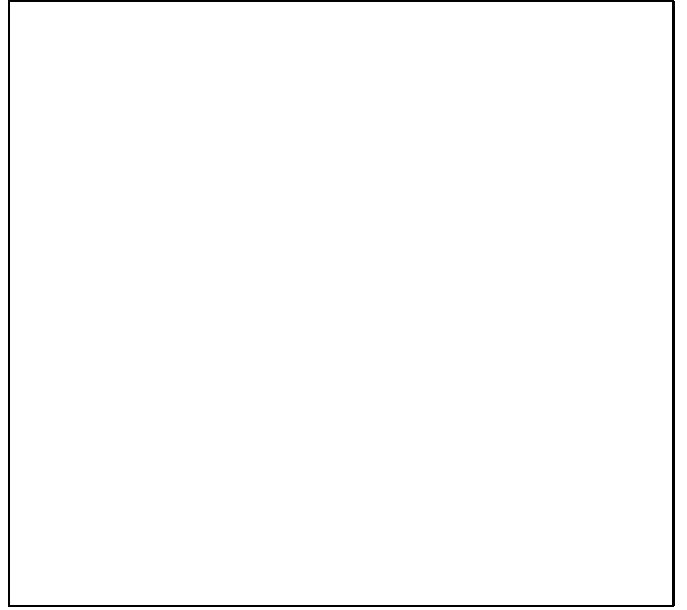


Fig. 3. Residuals of the X-ray fit overlaid with the R CCD image (zoomed image of $2' \times 2'$), with linear X-ray contours. The first contour is 9×10^{-7} counts s^{-1} arcsec $^{-2}$, and the step 4.1×10^{-7} counts s^{-1} arcsec $^{-2}$.

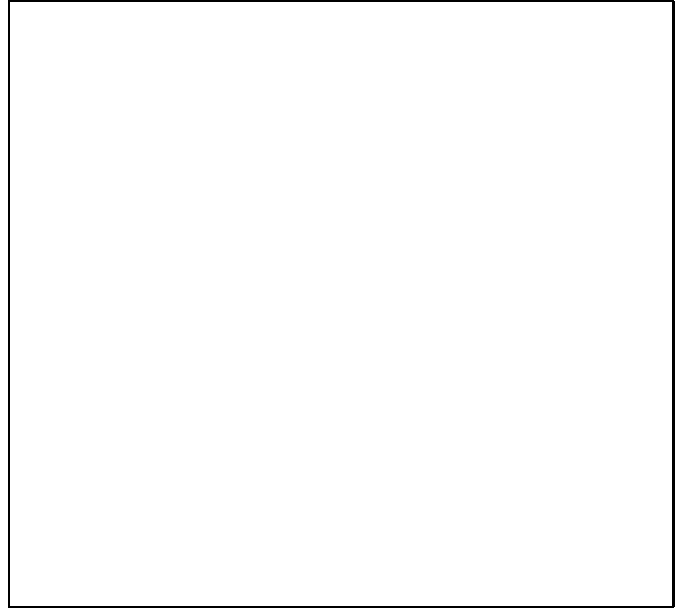


Fig. 4. Wavelet analysis of the central part of the X-ray map. Full line: scales of $5''$ (point-like sources); the two blobs P1 and P2 are visible, and located near the two galaxies labeled as in Paper II. Dotted line: contributions from scales of $20''$ which reveal, in addition to the central region, the diffuse clump S located beyond the arc. The first contour on both scales is at least 3σ above the local fluctuations; X-axis and Y-axis are in decimal degrees.

and elongated in the N-S direction. This excess of emission has a direction nearly perpendicular to the main orientation of the cluster, and the brightest part coincides with the cD position. However, the small number of photons available does not allow to assess whether this can be made of two point sources. In order to check the reality of its elongated shape, we produced two sub-images selecting photons according to their arrival time on the detector, half photons in each image. The N-S elongation remains in both sub-images, and thus can be considered as real.

The two blobs P1 and P2 deserve also some comments. First, we notice that the position of P2 is consistent with that of galaxy #364, a “normal” elliptical galaxy at redshift $z=0.2334$ (Paper II). P2 is by far the brightest signal, after the cluster core, observed at this scale over the whole cluster extent. A possible interpretation could be X-ray emission originating from hot gas trapped in a dark matter halo associated to the galaxy #364. The second blob on the other side of the cD, P1, is also located near the galaxy #314, likely to be a cluster member. But in both cases, the residual uncertainty of a few arcseconds in the X-ray/optical alignment leaves room for alternative explanations and the coincidence with the underlying galaxies could well be fortuous. Thus, another interpretation of these small scale structures could relate them to the presence of the cooling flow. As suggested above, there may be some inhomogeneities in the dark matter distribution, and the infalling gas can be trapped in secondary potential wells such as P1 and P2. Moreover, if the infalling gas is cooler and denser than the surrounding medium, it has a higher X-ray emissivity in the ROSAT band and may be easier to detect. One striking point is the global alignment of P1 and P2 with the main elongation of the cluster and the nearly perfect alignment with the central X-ray emission. This kind of features has already been detected in two well-known cooling flow clusters, namely A85 and A496 (Prestwich et al. 1995). In these two clusters, some residuals are detected in the central region of X-ray emission, possibly unresolved at the ROSAT HRI resolution, and with typical intensities of 3 to 10×10^{41} ergs s^{-1} and distances to the center of 10 – 15 kpc. In the case of A2390, the corresponding values are of the order of 10^{42} ergs s^{-1} and 50 kpc, slightly larger. They may reflect the intensity of the cooling flow, as discussed below.

On scales of $20''$ the contribution from the cluster center is still large, but a significant emission is again found some $40''$ from the center, definitely confirming the presence of the diffuse component S of X-ray emission located beyond the giant arc.

2.3. Optical observations and galaxy distribution

In order to compare the X-ray map to the light distribution of the cluster, a photometric catalog of the galaxies was produced from deep images of the cluster in B and R, covering a larger field than the images analysed in Paper II and best suited to the extent of the X-ray image. The CCD images were obtained in the course of a systematic deep imaging of cluster-lenses performed in collaboration with J.A. Tyson and collaborators, at the Kitt Peak 4 meter telescope in August 1989. Images were obtained, with the B_J and the R filters, for which the photometric system is defined in Gullixson et al. (1995). The details of the photometric analysis of the cluster will be published elsewhere (Tyson et al., in preparation), but we can shortly sum-

marize here the main characteristics of the observations. The field of view is $8' \times 8'$ with a pixel size of $0.47''$ and a seeing on each final image of $1.2''$. The total exposure time was $2h\ 20mn$ in R and $4h$ in B_J , giving a detection level of $\mu_R = 27.5$ and $\mu_J = 28.3$ at a 1σ level. Photometry of the field was performed using the standard FOCAS routines (Valdes et al. 1983). We estimate the completeness limit of the final catalog to $R = 23.8$ and $B_J = 26$, with more than 1200 objects within this limit. For the purpose of the present paper, we derived two maps from this catalog, namely the map of isoluminosity contours and the map with isopleth contours. Selection criteria were used in order to reduce the contamination by non-member objects. First, only the objects classified “galaxy” by the FOCAS classification scheme were kept in the catalog. We also cut the catalog down to its completeness limit ($16.9 < R < 23.8$) and introduced a color selection ($1.5 < B_J - R < 2.5$, with color indices computed in the B_J isophote) as the sequence of the ellipticals falls in this range in the color-magnitude plot. This selection allows a significant reduction of the statistical noise introduced by the star contamination. Our final working sample contains 517 objects. Each map was computed on a regular grid of points every 10 pixels, with the method developed by Dressler (1980), *i.e.* the radius of the 10th most distant object from each grid point defines the integration surface. The accuracy in the determination of the maximum of the map is about 1 grid point, or $5''$ on the final map. A smoothing with a gaussian filter 25 pixels wide was applied, giving a resolution of $12''$, similar in average to the X-ray map.

If we assume that the X-ray distribution follows the gas density distribution, we can also compare this distribution with the galaxy distribution. As seen in Fig. 5, the optical luminosity distribution coincides with the X-ray centroid and is strongly dominated by the central cD. On the contrary, the isopleth map is less convincing in the sense that there is no strong overdensity of objects near the center, probably because of an antisegregation effect, *i.e.* a default of galaxies near the giant one, due to cannibalism effects and dynamical evolution in the cluster core. Moreover, there is a global elongation of the cluster in the direction -50° from the N-S axis, similar to the X-ray map. The ellipticity of the luminosity map is typically of $b/a \sim 0.7$, again similar to the large scale ellipticity of the X-ray. This result can be compared with the analysis of 5 Abell clusters proposed by Buote and Canizares (1992) who find, contrary to this cluster, a significant disagreement between the X-ray ellipticities and the galaxy distribution. Projection effects on the ellipsoid may be one reason for this discrepancy. The alignment of the cD along the privileged direction can also be noticed, as it is the case in many cD clusters. Finally, one may note that the galaxy distribution is more clumpy than the X-ray, in particular at larger distances. Indeed at least two clumps of galaxies located on each side from the center are clearly visible in Fig. 5, but do not show significant counter-parts in the X-ray map. They probably correspond to some subcluster components interacting with the much more evolved main potential, which was able to accumulate the hot gas since its formation.

2.4. Existence of the X-ray sub-structure “S”

From the X-ray emission of the NW sub-structure, we can roughly estimate its contribution to the total mass. As written above, the X-ray luminosity is roughly 100 times lower than

the total one so this corresponds to an associated “velocity dispersion” 5 times smaller than the central one, if we assume that the X-ray luminosity varies as σ^3 (Edge & Steward 1991). The mass is also assumed to vary as σ^2 , which is exact in the case of an isothermal mass distribution, and can be considered as a first order approximation otherwise. So the mass associated to the sub-structure is about 20 times smaller than the cluster mass, a rather standard value for sub-structures associated to rich clusters of galaxies. The definite confirmation of its dynamical existence would be to detect a secondary clump in the velocity histogramme of cluster members. But as shown, its width would be only 3 to 5 times smaller than the main distribution. Moreover, from Paper II, the redshift for the main galaxy of the clump (# 388, the galaxy near the arc) is 0.231, or a zero radial velocity with respect to the cD. A possible sub-component in the histogram would be centered roughly at the same redshift as the main one! The velocity histogramme issued from the spectroscopic survey analysed in Paper II shows a positive kurtosis which could be interpreted as the addition of a gaussian with a width of 600 km s^{-1} on the main gaussian, 2000 km s^{-1} wide. Indeed the galaxies in the bin $\pm 600 \text{ km s}^{-1}$ are highly concentrated near the cluster center, in a region including the clump “S”, while the galaxies having higher radial velocity have a smoother distribution over the cluster. This might be a further evidence for the dynamical reality of the clump, although it is difficult to spatially separate the two samples.

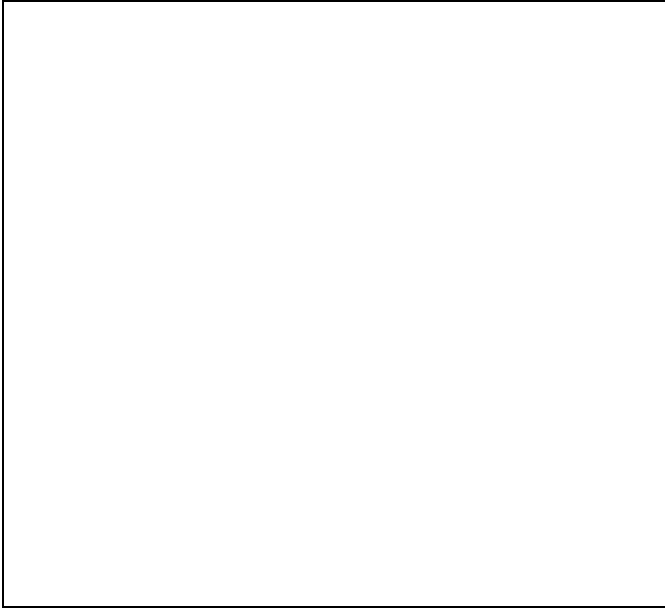


Fig. 5. Luminosity density contours overlaid on the R image of A2390. The map was smoothed to give a typical resolution of $12''$, similar to the large scale distribution of the X-ray gas.

3. Analysis of the X-ray flux and profile

3.1. X-ray profile

Because of the significant elongation of the cluster, elliptical coordinates are the best adapted for the determination of the brightness profile (Buote and Canizares 1992, 1994). Since the ellipticity parameters vary with the radial distance,

we adopted mean values corresponding to a region where the surface brightness has decreased by a factor of 2 to 3 from its central value (i.e. a major axis of $\sim 50''$); this yields $b/a = 0.74$ and $PA = -51^\circ$ (same definition as in Fig. 2).

After the image transformation, photons were binned into concentric rings and the resulting surface brightness profile is displayed in Fig. 6. A King model

$$S(R) = S_0(1 + (R/R_c)^2)^{0.5-3\beta} + bkg$$

was fitted to the data, introducing simultaneously to the fit a deconvolution by the HRI PSF (David et al 1992). The overall profile is extremely steep and leaves the innermost points in excess as the signature of the cooling flow when the fit is extended out to $500''$. A tractable analytical expression for the profile was obtained by fitting a King model only up to the point where the profile reaches the background level, *i.e.* a radius of about $250''$. With this restriction the fit was satisfactory, giving $\beta = 0.41$ and $R_c = 7.0''$ for $0 < R < 250''$ and a background value of $1.15 \cdot 10^{-6} \text{ counts s}^{-1} \text{ arcsec}^{-2}$. To check the validity of our assumption, we computed the expected 2D surface brightness taking a 3D gas density given by:

$$n(r) = n_0(1 + (r/R_c)^2)^{-3/2\beta} \quad \text{for } 0 < r < 250''$$

and

$$n(r) = 0 \quad \text{for } r > 250''$$

using the above values for β , R_c and the background level. The modelled surface brightness convolved by the HRI PSF is shown on Fig. 6 in comparison with the observed profile and appears to be fully satisfactory. The corresponding density will be adopted in the rest of the paper. For this calculation, we have implicitly assumed that the observed surface brightness is weakly dependent on the gas temperature, which is justified, according to the expected high temperature (even in the cooling flow region) of this very bright cluster, and the poor temperature sensitivity of the ROSAT HRI above 5 keV. Moreover, this very uncommon combination of β and R_c should not be ascribed any physical meaning, but is only indicative of the presence of cooling flow, its main advantage being to allow a straightforward derivation of the density profile.

3.2. Total luminosity

The cluster luminosity was calculated integrating counts up to a maximum radius and corrected with the background value determined above. Corresponding count-rates were converted into luminosity using a Mewe-Kaastra thermal model folded with the HRI response provided by the EXSAS package. Assuming a thermal spectrum of 9 keV (cluster average temperature), a heavy element abundance of 0.5 in solar units and taking a galactic neutral hydrogen column density at the cluster's position of $N_H = 6.7 \cdot 10^{20} \text{ cm}^{-2}$ (Dickey & Lockman 1990), we obtain respectively

$$Li = 5.63 \cdot 10^{44} \text{ h}^{-2} \text{ ergs s}^{-1} \quad \text{for } Ri = 250''$$

$$Lo = 6.30 \cdot 10^{44} \text{ h}^{-2} \text{ ergs s}^{-1} \quad \text{for } Ro = 400''$$

in the 0.1-2.4 keV band depending on the radius of the integration limit for the total flux. This is significantly higher than the Einstein luminosity ($L_X = 3.85 \cdot 10^{44} \text{ h}^{-2} \text{ ergs s}^{-1}$ in the range 0.7-3.5 keV, Ulmer et al. 1986); the difference is too large to be

attributed to the influence of the cooling flow only, although the ROSAT band is softer than Einstein, and results presumably from an error in the analysis of the Einstein data (as it is also the case for the very bright cluster A2163, Elbaz et al. 1995). Fig. 6 also shows that R_0 is a conservative boundary for the flux integration; however, because of the absence of profile modelling beyond $250''$ and the rather high background of the HRI, it is difficult to estimate how far the cluster emission actually extends, and consequently apply any correction for the total luminosity. Normalizing the density profile according to Li , we obtain $n_0 = 5.7 \cdot 10^{-2} \sqrt{h} \text{ cm}^{-3}$ which is unusually high. Using the Temperature - Luminosity relation (Henry & Arnaud 1991) we derive a temperature of $\sim 9 \text{ keV}$. This is however only indicative, for the dispersion in the empirical relation is large mostly because of possible cooling flows. Having no observational constraints on temperature, we shall adopt this value as the mean cluster temperature in the following.



Fig. 6. Surface brightness profile. A bin size of $2.5''$ was used in order to have a central annulus of $5''$ diameter to fully exploit the HRI resolution. The solid line is the best fit obtained assuming a King density profile truncated at $R=250''$ (see text)

3.3. Evidence for a strong cooling flow

In this section, we propose to estimate the cooling radius and the mass flow rate in this cluster. Since the electron density scales as \sqrt{h} and the time as h^{-1} , these quantities are not simple functions of h and we give a detailed calculation in the two cases: $h = 0.5$ and $h = 1$. The cooling time as a function of density may be estimated by (Henry and Henriksen 1986):

$$T_{cool}(yr) = 6 \cdot 10^{10} \left(\frac{T}{10^8 K} \right)^{1/2} \left(\frac{\rho}{10^{-3} \text{ cm}^{-3}} \right)^{-1}$$

Using the density profile determined above and assuming again a temperature of 9 keV , we derive R_{cool} defining the region where the cooling time is smaller than the age of the universe at the cluster redshift ($t_{univ} = h^{-1} 10^{10} (1+z)^{-3/2}$). This gives $R_{cool} = 43''$ (200 kpc) for $h=0.5$ and $R_{cool} = 32''$ (75 kpc) for

$h=1$. Calculating the bolometric cluster luminosity enclosed within this radius (L_{cool}) and assuming a steady state isobaric gas cooling from 9 keV , we derive the mass flow (Fabian et al. 1991):

$$\dot{M}_{cool} = \frac{2}{5} \frac{\mu m_p}{kT} L_{cool} \sim 880 \frac{L_{cool}}{10^{45}} \left(\frac{T}{5 \text{ keV}} \right)^{-1} M_{\odot} \text{ yr}^{-1}$$

This yields $\dot{M}_{cool} \sim 850 M_{\odot} \text{ yr}^{-1}$ or $\dot{M}_{cool} \sim 180 M_{\odot} \text{ yr}^{-1}$ for h equals 0.5 and 1 ; the fraction of the total luminosity enclosed within the cooling radius being $\sim 1/4$ and $1/5$ respectively. It should be also noticed that if a standard cooling time of $2 \cdot 10^{10}$ years is used (e.g. Edge et al. 1994), the mass rates are to be increased by $\sim 30\%$. Although uncertainties are large (up to a factor of ~ 2 , Fabian et al. 1991), the derived mass flow is amongst the highest rates ever observed (Edge et al. 1994). Similar values can be derived from the analysis of the optical data (Paper IV).

4. X-ray and lensing constraints on the gravitational potential

4.1. Modelling constraints

Multiple images modelling have successfully demonstrated that the mass distribution in the central part of clusters of galaxies is centered on the brightest cluster galaxy (BCG) with an orientation and ellipticity comparable to the orientation and ellipticity of the halo of the BCG. Moreover, the core radius of the mass distribution is found to be very small ($20\text{--}50 h^{-1} \text{ kpc}$), not only in the case of cD-type cluster (MS2137: Mellier et al. 1993; A370 and A2218: Kneib et al. 1993, 1995), but also in clusters with multiple galaxies in the center such as Cl0024+17 (Smail et al. 1995b). These studies show also that the overall matter distribution is clumpy. Kneib et al. (1993) found that the mass distribution in A370 is bimodal, a result that has been confirmed by the ROSAT/HRI image of this cluster (Fort & Mellier 1994). In the case of A2218 (Kneib et al. 1995) it is also necessary to add some other clump of mass on the second brightest galaxy of the cluster despite no sub-structure is resolved on the deep ROSAT/HRI image.

Previous lensing model of the straight arc in A2390 were done in Paper I and by Kassiola, Kovner & Blandford (1992) and Narasimha & Chitre (1993). These studies however do not reflect the ROSAT/HRI observations, in particular the lip-caustic model of Narasimha & Chitre (where the center of the mass distribution is very close to the straight arc) and the unrealistic fold model and beak-to-beak model with two identical large masses (see Figures 6 & 7 of Kassiola et al.). Their beak-to-beak model with a marginal cluster and two small masses (their Fig. 8) is probably the closest to the X-ray observations. However the overall ellipticity and orientation of their main clump is incorrect, and their model needs fine tuning to reproduce the straight arc.

The detection of the NW sub-structure “S” in X-ray allows us to put strong constraints on the location of the secondary deflecting mass and its intensity relative to the main peak in the construction of the global gravitational potential. Therefore the measured distortion and orientation of the straight arc allows to calibrate the absolute central mass distribution. The clump acts as a perturber as shown in Paper I and locally enhances the convergence and the shear. The shear direction is then almost straight around the perturber if it has a somewhat

smooth mass distribution (with a core size of the order of at least the size of the straight arc - which is not the case of the preferred model of Kassiola et al.).

To quantify the amount of mass in the central part we have done a simple mass model taking into account the above considerations, as well as the geometrical constraints coming from the X-ray luminosity map. Indeed, the lensing constraints are relatively poor in this cluster, since no multiple images are identified; thus, in order to constrain the mass model, we had to fix some parameters of the mass distribution. We shall show here that a mass model defined with two clumps of mass (the main one centered on the cD galaxy and the other one centered on the “sub-structure”) is compatible with both the X-ray data and the lensed features. A single clump lens-model cannot reproduce the observed lensed image unless it is not centered on the cD galaxy and has a core much larger than the ones found in other cluster-lenses. Adding a second clump of mass with a core of the size of the straight arc will generate locally a flat mass distribution that will have an almost constant convergence and shear direction, and therefore will produce highly amplified arcs and arclets, straight and parallel, as expected from the optical observations of Paper I.

The density profile used is the one of Kassiola and Kovner (1993) of the form:

$$\Sigma(R) = \Sigma_0 \frac{R_C}{\sqrt{R_C^2 + R^2}}$$

We fixed the ellipticity and orientation of the main clump to be the ones of the cD halo or the X-ray map at a typical radius of $50''$ namely $b/a = 0.7$ and $PA = -49^\circ$. In order to be consistent with the results found in previous cluster-lenses (see discussion above) we fixed the core radius of the central clump to be $R_C \approx 13''$ ($30 h^{-1}$ kpc). For the secondary clump we assume for simplicity a circular shape and a core radius of the same order ($7-12''$). Therefore there are only two unknown parameters, namely the central mass density of both clumps. These are easily constrained by the shape and orientation of the straight arc as well as the shear direction in that region. The straight arc puts strong upper limits on the overall mass as it has no counter image candidate and thus limit the extension of the critical line up to its position. It also gives a lower limit of the mass as it needs to be well magnified for an object at redshift 0.913 (Paper I). Table 2 gives the fiducial mass model which is compatible with the straight arc and the shear around it. Figure 7 shows the predicted shear map around the cluster center.

Quantitatively, the projected mass we find in a circle of radius $38''$ or $88 h^{-1}$ kpc, corresponding to the distance of the arc is: $M_{tot}(< R_{arc}) = 0.8 \pm 0.1 \cdot 10^{14} h^{-1} M_\odot$. The integrated luminosity inside the same surface has been computed in the photometric catalogue including only the “galaxies” but with no color selection. We also added a k-correction of 0.242. Finally, the total luminosity is $L_{Rtot}(< R_{arc}) = 3.0 \pm 0.1 \cdot 10^{11} h^{-2} L_\odot$, and the corresponding mass-to-light ratio is $M/L_R \simeq 260 \pm 40 h$ (M/L) $_\odot$. The velocity dispersion inferred from the lensing model (Table 2) is about twice smaller as the value published in Paper II, but is consistent with the lower σ_v found within the central region of the cluster and discussed in Sec. 2.4.

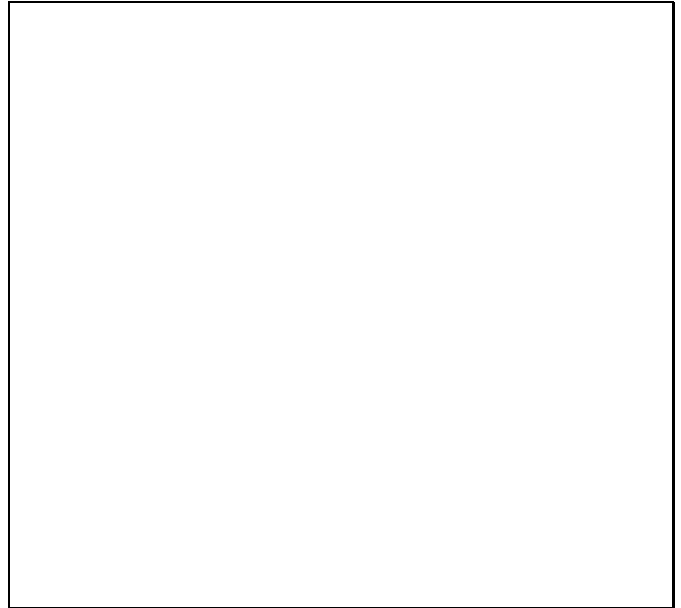


Fig. 7. Results of the lensing model overlaid on the optical image of A2390. The contours represent the mass distribution and the sticks the direction and amplitude of the shear at redshift 0.913, *i.e.* the giant arc redshift.

4.2. Dark matter and cooling flow

In the rest of the paper, we assume a Hubble constant of 50 km/s/Mpc for the sake of clarity in the comparison with other observations and numerical simulations.

It is usually impossible to infer constraints on the temperature of clusters of galaxies when no X-ray spectral information is available, and one is usually left with the temperature estimate provided by the L_X - T relation (cf Sect. 3.2). But in the case of A2390, the presence of the giant gravitational arc provides an elegant alternative to classical temperature measurements, in the sense that it strongly constrains the shape and the strength of the underlying potential (at least for the central part). In the hypothesis of hydrostatic equilibrium (which is justified, since cooling flows are supposed to be highly subsonic), the derivation is straightforward.

The 3D mass distribution derived from the projected mass density used in the lensing simulation is:

$$m(r) = m_0 f(x)$$

where

$$x = r/R_C, \quad f(x) = x - \arctan(x), \quad m_0 = 4\pi\rho_0 R_C^3$$

Replacing by the numerical values, *i.e.* $R_C = 13''$ and the total projected mass enclosed within $R_{arc} = 38''$ ($0.8 \cdot 10^{14} h^{-1} M_\odot$), we find $m_0 = 2.35 \cdot 10^{13} h^{-1} M_\odot$. Then, assuming that the potential is well represented by the lensing mass profile extrapolated up to the radius where diffuse gas emission is observed, we can solve the hydrostatic equilibrium:

$$\frac{1}{\rho} \frac{dP}{dr} = -\frac{Gm_0}{r^2} f(x)$$

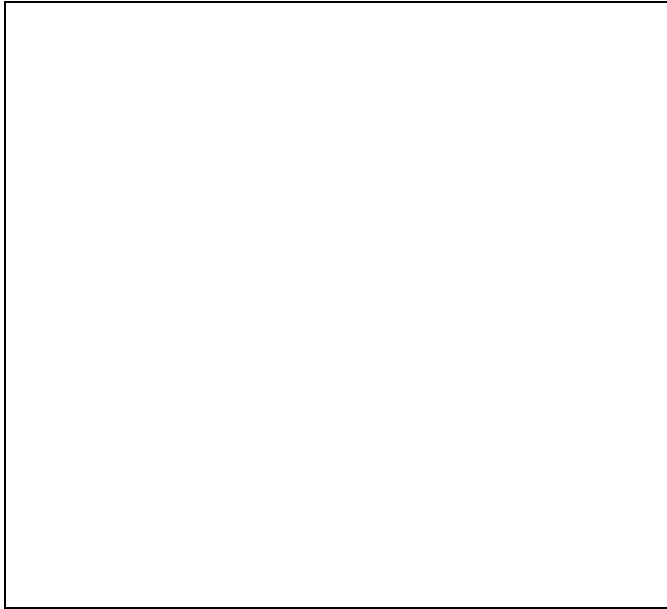
assuming an ideal gas

$$\rho(r) = m_p n(r) \mu \quad P = nkT$$

Table 2. Fiducial parameters of the two projected potential found for the best model of the arc.

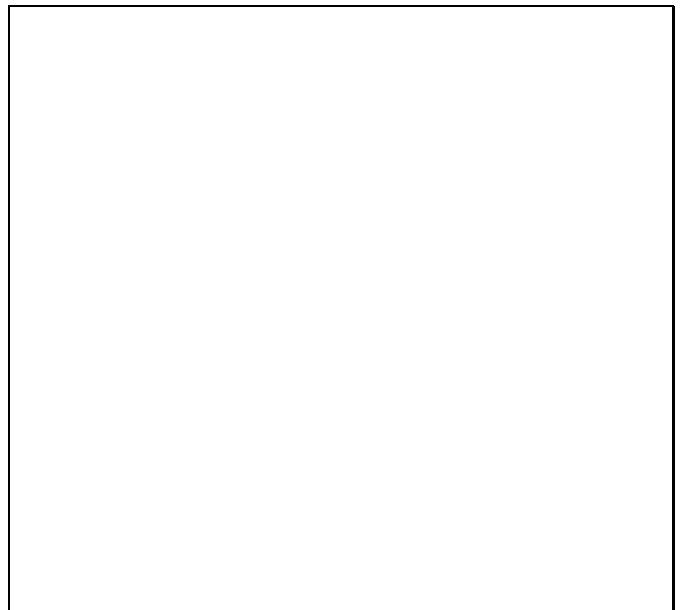
	x_c (")	y_c (")	ϵ $\frac{a^2-b^2}{a^2+b^2}$	b/a	PA	R_C (")	σ_∞ km s ⁻¹	$M_{tot}(< R_{arc})$ $10^{14} h^{-1} M_\odot$
cD clump	0.	0.	0.3	0.71	49.2°	12±5	950±100	0.8±0.1
sub-clump	42±2	10±5	—	—	—	7–12	420–500	—

The equation was integrated taking the gas density, $n(r)$, derived in Sect. 3.1 and an outside temperature of 9 keV, as boundary condition.

**Fig. 8.** Full line: cluster profile temperature calculated assuming the gravitational potential derived from the lensing analysis (independent of H_0). The dotted and dashed lines correspond respectively to models where either the gravitating mass has been divided by 2 or the lensing radius multiplied by 2.

The corresponding temperature profile is displayed on Fig. 8 (solid line), showing a significant temperature drop toward the center as well as a negative temperature gradient beyond $\sim R_{arc}$. Although this is perfectly plausible with the cooling flow picture, it is difficult to estimate the uncertainty on the profile. Assuming a higher outside temperature flattens the outer temperature gradient but leaves T_{max} almost unchanged. On the other hand, one can certainly explore the influence of the lensing parameters. Two alternatives modifying the lensing constraints have been investigated: (1) $m_o \rightarrow m_o/2$ and (2) $R_C \rightarrow 2R_C$; the corresponding temperature profiles are also presented on Fig. 8. The resulting profiles are also consistent with a cooling flow scenario, but show significantly different inner temperatures. The values chosen for these alternatives are, however, *excluded* from the lensing analysis and it clearly appears that it would be extremely difficult to constrain further the temperature profile of this distant cluster. Technically, it is very unlikely that present day spatially resolved X-ray

spectroscopy may discriminate between the different possibilities (ASCA has only a spatial resolution of $\sim 3'$). But the forthcoming XMM, with a resolution of $\sim 30''$ may be able to verify these results. Anyway, a single observation with ASCA should provide a good estimate of the cluster mean temperature, which is one of the main unknown of the problem.

**Fig. 9.** Integrated total mass profile (full line) and gas mass profile (dotted line). At $R = R_{arc} = 38''$, the gas fraction represents only $\sim 1/35$ of the total mass. (computed for $H_0=50$, M_{tot} scales as h^{-1} , M_{gas} as $h^{-2.5}$)

The other source of uncertainty is the potential shape at large radial distances. In the hypothesis where the analytical expression of the lensing potential holds up to the cluster periphery, we have computed the integrated mass (gas mass and total mass) as a function of radius (Fig. 9). At the radial distance of the giant arc, the gas represents only $\sim 1/35$ of the total mass, whereas at $250''$ this fraction reaches $1/12$. This last value is in agreement with what was found previously in rich clusters (Böhringer 1994), but needs to be confirmed with a proper definition of the cluster potential beyond the giant arc (e.g. using weak shear methods). On Fig. 9, it is also conspicuous that the dark matter is more concentrated than the gas distribution, despite the presence of the cooling flow.

With the above temperature profile a direct analytical expression of the mass flow rate can be derived, using the equa-

tion of energy conservation:

$$\rho v \frac{d}{dr} \left[\frac{v^2}{2} + \frac{5}{2} \frac{kT}{\mu m_p} + \Phi \right] = n^2 \Lambda T^{1/2}$$

Taking the lensing gravitational potential, the derived temperature profile, a cooling constant $\Lambda = 1.63 \cdot 10^{-27} \text{ cgs}$ (corresponding to the cooling time used above) and neglecting the quadratic velocity term, we find a mass flow rate:

$$\frac{dM}{dt} = 4\pi r^2 \rho v$$

of $\sim 710 M_\odot \text{ yr}^{-1}$ for a cooling radius of $43''$ which is in very good agreement with the estimate obtained in Sect. 3.3 and confirms the presence of a massive cooling flow in the center of A2390.

5. Discussion and conclusions

Throughout this study, Abell 2390 appears to be one of the most distant cluster of galaxies for which a detailed analysis enabled the discovery of an unvalued collection of remarkable properties: high velocity dispersion, presence of a peculiar gravitational arc, preferential direction strongly underlined both by optical and X-ray data, high X-ray luminosity, massive cooling flow, presence of sub-structures. The purpose of this paper was the analysis of a high resolution X-ray image in close connection with optical informations. Thanks to the large number of X-ray photons available, it was possible to take advantage of the maximal resolution provided by the ROSAT HRI and study the core of this cluster down to scales of $5''$ i.e. $\sim 12 h^{-1} \text{ kpc}$. The combination of X-ray and optical observations allowed to bring a coherent picture of the cluster under the very simple hypotheses of hydrostatic equilibrium and that “light traces mass”, at least in its ellipticity and its orientation.

Two main new results have to be highlighted, for they have numerous consequences as to the dynamical state, and thus the formation processes of this massive cluster as suggested by various numerical simulations: (i) a high X-ray luminosity partly caused by a strong cooling flow ($\sim 250 h^{-2} M_\odot \text{ yr}^{-1}$) and having an elliptical morphology on large scales. (ii) The presence of a diffuse sub-structure playing a key role in the modelling of the lensing constraints. We now briefly discuss our findings.

In addition to the sub-structure which is best seen on scales of the order of $20''$, two point-like contributions were detected as well as a strong emission from the cluster core. The latter is significantly elongated in a direction perpendicular to the cluster main orientation, however not spatially resolved in width in the HRI data. It is interesting to notice that the inner core of A2218 seems to present the same “counter-alignment” property (Kneib et al 1995). Apart from this, it is remarkable that all the sub-structures, together with the filament observed in the optical and the giant arc are well aligned along the direction defined by the cD main axis, which is also suggested by the galaxy distribution on larger scales. The overall cluster X-ray morphology is moreover strongly elliptical, with the major axis also coinciding with the cD’s, even though the ellipticity parameters are somewhat varying with radial distance. Such alignments - at least between X-ray shape and cD orientation - seem to be quite a common property of relatively bright X-ray clusters (e.g. Edge et al. 1994; Pierre et al. 1994) and are

probably related to the way they formed. Indeed, recent 3D hydrodynamical simulations (Katz & White 1993), leading to the formation of a Virgo type cluster as to the final mass (we find for A2390 a mass of $\sim 10^{15} M_\odot$ within 1.2 Mpc) in a CDM model with $\Omega_b = 0.09$, shows that filaments begin to form by $z \sim 0.4$. Dark matter halos continue to “condense” out of the filaments; material can flow large distance (over 11 Mpc) along the filaments to reach the forming cluster, while the material that falls into the cluster without flowing down a filament is of much more local origin. This gives the general impression that cluster formation occurs by flow along a set of intersecting filaments rather than by quasi spherical collapse. The fact that A2390 presents strong alignment properties supports very well this picture. Katz & White simulations show moreover that the intra-cluster medium is far from isothermal: in addition to a central cooling flow, the temperature falls with radius throughout the virialized region of the cluster. This is qualitatively in perfect agreement with our X-ray analysis if we assume that the potential shape, constrained by the lensing up to $\sim 40''$ holds at much larger radial distances.

A recent X-ray analysis of the simulated Katz & White clusters by Buote & Tsai (1995) provides interesting assessments as to the actual validity of such a study where one attempts to derive the dark matter profile from the X-ray luminosity distribution under the hypothesis of hydrostatic equilibrium. Generally speaking, in order to generate the same ellipticity of the potential at a given distance, a cluster having a negative temperature gradient for the X-ray emitting gas will have to be more elongated than a cluster having an isothermal gas. They find that conclusions regarding the shape of the dark matter are not overly sensitive to the temperature gradient of the gas. In particular, for redshifts between 0.25 and 0.13 there is an excellent agreement between the X-ray and true dark matter shapes provided that the true inclination of the cluster is taken into account; otherwise the deviation from the true ellipticity increases considerably. This is undoubtedly one of the major limitations of the present study but, owing to the internal consistency of our results and the apparent strong elongation of the cluster, we are confident that the symmetry axis of the cluster should be within $\pm 30^\circ$ from the plane perpendicular to the line of sight. The presence of the giant arc in A2390 allowed to infer the shape of the dark matter distribution with an independent method. Surprisingly, all the distributions (X-ray gas, dark matter, galaxies) present the similar ellipticities, reinforcing the conclusions discussed here.

Finally, the extended structure discovered in the X-ray emission agrees well with what was expected for producing the exceptional shape of the giant arc, namely the presence of a secondary deflecting mass located beyond the arc and aligned with the cD-arc axis as already suggested in Paper I. On the qualitative point of view, it is worth underlying the analogy between the distribution of matter that we observed around the arc and Kassiola et al. (1992) “preferred model” (e.g. their Fig. 8). Although their numerical solution does not match exactly our findings, their general idea should be regarded as valuable. Such a distribution of matter predicts, however, that the giant arc should be made of two galaxy images, a fact which is corroborated (as noticed by Kassiola et al.) by the infrared observations of Smail et al. (1993). Further HST observations will most probably disentangle the uncertainties on the morphological shape of the source of the giant arc. It is worth noting that similar X-ray/optical studies of cluster-lenses have

already brought some indications on the dynamical state of rich clusters of galaxies. In particular, in the clusters A370 and A2218, the lens modellings have revealed significant departures from the virialised state, in agreement with the irregularities of the X-ray maps (Kneib et al. 1995). On the contrary in the case of A2390, the gas distribution is more regular, and dominated by a massive cooling flow a phenomenon which can appear only if the dynamical secular evolution is far from violent, and is destroyed during merger phases for example. This is a valid argument to understand why this cluster appear rather regular in its X-ray distribution.

In this paper, we have only discussed the matter distribution of the cluster on its central regions. More extended analysis will benefit from a weak shear approach, *i.e.* the large scale statistical analysis of the gravitational deformations. Recent theoretical works have proposed different methods to invert the shear map to recover the mass distribution (Kaiser & Squires 1993, Seitz & Schneider 1995). Detection of the weak deformation on the faint background population at the periphery of the clusters (Bonnet et al. 1994; Fahlman et al. 1994; Smail et al. 1995c) are very promising, as they should provide strong constraints on the slope of the mass profile. The mass estimated by this technique seems presently quite large (Bonnet et al. 1994; Fahlman et al. 1994), but the uncertainties are large too and critically dependent on the quality of the observations. The future comparison between these mass maps and the mass derived from large scale X-ray distribution such as those from ROSAT/PSPC data will be important to confirm the apparent increase of dark matter outside the central regions of rich clusters of galaxies. If these results are confirmed, it could have important cosmological implications.

Acknowledgements. We wish to thank Y. Mellier and R. Pelló for their constant interest in this work and all their comments on this paper, B. Fort, G. Mathez and A. Blanchard for interesting discussions on clusters of galaxies, lensing and gas dynamics and M. Arnaud for the use of her plasma codes. We are also grateful to J.L. Starck for detailed informations on the wavelet analysis and the use of his package. JPK is grateful for financial grant from the EC HCM Network CHR-X-CT92-0044. This work was supported by the French Centre National de la Recherche Scientifique (INSU) and the Groupe de Recherche "Cosmologie".

References

- Allen S.W., Fabian A.C., Kneib, J.P., 1995, submitted
- Böhringer H., 1994, in "Cosmological aspects of clusters of galaxies", p 123, ed. Seitter, NATO ASI, Kluwer
- Bonnet H., Mellier Y., Fort B., 1994, ApJ 427, L83
- Buote D. A., Canizares C. R., 1992, ApJ 400, 385
- Buote D. A., Canizares C. R., 1994, ApJ 427, 86
- Buote D. A., Tsai J. C., 1995, ApJ 439, 29
- Daines S.J., Jones C., Forman W., Tyson J.A., 1995, preprint
- David L.P., Harden F.R., Kearns K.E., Zombeck M.V., 1992, U.S. ROSAT Science Data Center/ SAO, *The ROSAT High Resolution Imager*
- Dickey J.M., Lockman F.J., 1990, ARAA 28, 215
- Dressler A., 1980, ApJS 42, 565
- Edge A. C., Stewart G.C., 1991, MNRAS 252, 428
- Edge A. C., Fabian A. C., Allen S. W., Crawford C. S., White D. A., Böhringer H., Voges W., 1994, MNRAS 270, L1-L5
- Elbaz D., Arnaud M., Böhringer H., 1995, A&A 293, 337
- Fabian A.C., Nulsen P.E.J., Canizares C.R., 1991, A&AR 2, 191
- Fahlman, G. G., Kaiser, N., Squires, G. and Woods, D., 1994, ApJ, 437, 56
- Fort B., Mellier Y., 1994, A&AR 5, 239
- Gullixson C.A., Boeshaar P.C., Tyson J.A., Seitzer P., 1995, ApJS 99, 281
- Henry J.P., Arnaud K., 1991, ApJ 372, 410
- Henry J.P., Henriksen M.J., 1986, ApJ 301, 698
- Jedrzejewski R., 1987, MNRAS 226, 747
- Kaiser N., Squires, G., 1993, ApJ 404, 441
- Kassiola A., Kovner I., Blandford R.D., 1992, ApJ 396, 10
- Kassiola A., Kovner I., 1993, ApJ 417, 450
- Katz N. White S.D.M., 1993, ApJ 412, 455
- Kneib J.P., Mellier Y., Fort B., Mathez G., 1993, A&A 273, 367
- Kneib J.P., Mellier Y., Pelló R., Miralda-Escudé J., Le Borgne J.F., Böhringer H., Picat J.P., 1995, A&A in press
- Le Borgne J.F., Mathez G., Mellier Y., Pelló R., Sanahuja B., Soucail G., 1991, A&AS 88, 133 (Paper II)
- Loeb A., Mao S., 1994, ApJ 435, L109
- Mc Millian S.L.W., Kowalski M.P., Ulmer M.P., 1989, ApJS 70, 723
- Mellier Y., Fort B., Kneib J.P., 1993, ApJ 407, 33
- Merrit D., 1987, ApJ 313, 121
- Merrit D., Saha, P., 1994, ApJ 409, 75
- Merrit D., Tremblay B., 1994, AJ 108, 514
- Miralda-Escudé J., Babul, A., 1995, preprint
- Narashima, Chitre, 1993, J. Ast. Astronomy 14, 121
- Pelló R., Le Borgne J.F., Soucail G., Mellier Y., Sanahuja B., 1991, ApJ 366, 405 (Paper I)
- Pierre M., Soucail G., Böhringer H., Sauvageot J.-L., 1994, A&A 289, L37
- Prestwich A.H., Guimond S.J., Luginbuhl C.B., Marshall J., 1995, ApJ 438, L71
- Seitz C., Schneider, P., 1995, A&A, in press.
- Slezak E., Durret F., Gerbal D., 1994, ApJ 108, 1996
- Smail I., Ellis R., Aragón-Salamanca A., Soucail G., Mellier Y., Giraud E., 1993, MNRAS, 263, 628
- Smail I., Hogg D.W., Blandford R., Cohen J.G., Edge A.C., Djorgovski S.G., 1995a, MNRAS submitted
- Smail I., Dressler A., Ellis R.S., Kneib J.P., Couch W.J., Sharples R.M., Oemler A., Butcher H.R., 1995b, in press.
- Smail I., Ellis R.S., Fitchett M.J., Edge A.C., 1995c, MNRAS 273, 277
- Soucail G., Arnouts S., Le Borgne J.F., Pelló R., Fraix-Burnet D., in preparation (Paper IV)
- Ulmer M.P., Kowalsky M.P., Cruddace R.G., 1986, ApJ 303, 162
- Valdes F., Tyson J.A., Jarvis J.F., 1983, ApJ 271, 431